Phonons and anomalous thermal expansion behavior of H_2O and D_2O ice I*h*

M. K. Gupta,[1] R. Mittal,[1,2] Baltej Singh,[1,2] S. K. Mishra,[1] D. T. Adroja,[3,4] A. D. Fortes,[3] and S. L. Chaplot[1,2]
[1]*Solid State Physics Division, Bhabha Atomic Research Centre, Mumbai, 400085, India*
[2]*Homi Bhabha National Institute, Anushaktinagar, Mumbai 400094, India*
[3]*ISIS Facility, Rutherford Appleton Laboratory, Chilton, Didcot, Oxon OX11 0QX, United Kingdom*
[4]*Highly Correlated Matter Research Group, Department of Physics, University of Johannesburg, Auckland Park 2006, South Africa*

(Received 23 March 2018; published 4 September 2018)

In order to identify and quantitatively analyze the anharmonicity of phonons relevant to the anomalous thermal expansion in the I*h* phase of ice, we performed neutron inelastic scattering measurements to study the phonon spectrum as a function of pressure up to 1 kbar at 225 K in deuterated ice (D_2O), and as a function of temperature over 10–225 K at ambient pressure in both H_2O and D_2O ice. We also performed density functional theory calculations of the lattice dynamics. The anomalous expansion is quantitatively reproduced from the analysis of the neutron data as well as from the *ab initio* calculations. Further, the *ab initio* calculations are used to visualize the nature of anharmonic phonons across a large part of the Brillouin zone. We find that the negative thermal expansion below 60 K in the hexagonal plane is due to anharmonic librational motion of the hexagonal rings of the ice molecules, and that along the hexagonal axis originates from the transverse vibrations of the hexagonal layers.

DOI: 10.1103/PhysRevB.98.104301

I. INTRODUCTION

Understanding the behavior of ice over a broad range of thermodynamic conditions is of great importance in the field of Earth and planetary sciences as well as in fundamental physics and chemistry [1–21]. Ice is known to exhibit polymorphic structures, depending on the environmental conditions [1]. It exists even in outer space, in comet clouds and interstellar grains [7–9]. The known phase diagram of ice is extremely rich [1]. The hydrogen bonds in ice are weak enough to be bent, stretched, or shortened substantially under pressure, which explains various crystalline structures that have been identified so far.

Ice has many anomalous properties and perhaps a most complex phase diagram. Ordinary ice (I*h*) crystallizes in an open structure which provides ample possibilities for rearrangements with pressure and temperature. The region of stability of ice I*h* has been extensively studied [1,12–14] both by experiments as well as theories. Among all the known crystalline ice phases, ice (I*h phase*) exhibits anomalous thermal expansion [12,13] behavior. It exhibits negative thermal expansion (NTE) at temperatures below ∼60 K. As temperature increases above 60 K, it shows a large positive thermal expansion coefficient. The understanding of the mechanism of the anomalous thermal expansion involves an understanding of the underlying dynamics of hydrogen-bonded water molecules in ice and their behavior on compression. Here we focus on one of the peculiarities, namely, the anomalous expansion behavior with temperature in ice I*h*. The thermodynamic stability of various phases of ice including the role of vibrational anharmonicity [2,14,19,20,22–33] have been studied by various groups. *Koza et al.* [15–17] reported extensive neutron and x-ray scattering experiments dedicated to the study of the dynamics of some high-density crystalline and amorphous ice structures. Spectroscopic studies have been reported using dielectric, infrared (IR), Raman, and neutron measurements [21,34–37]. Strassle *et al.* [14] have measured the pressure dependence of low-energy phonon dispersion in deuterated ice (D_2O) to understand the pressure-induced amorphization and NTE behavior. The measurements along the high-symmetry directions in the Brillouin zone show softening of low-energy modes of about 5–7 meV. The phonon density of states of H_2O and D_2O ice in the I*h* phase [38] has been measured at 15 K. Edgar *et al.* [20] theoretically studied the significance of phonon anharmonicity on the stability of hexagonal ice over the stability of cubic phase. The isotope effect of H and O on ice volumes has been studied by various authors [3,4,39,40]. The effect at low temperature has been related to low-energy phonons linked to the hydrogen bonding network. Others studies on ice addressed the proton hopping/disorder and diffusion in ice using dielectric and quasielastic neutron-scattering method [21,41].

Since the mechanism of the anomalous thermal expansion involves anharmonic phonons over the entire Brillouin zone, it is necessary to study the complete phonon spectrum. Similarly, there is a need to investigate the anharmonicity and phonon eigenvectors across the entire Brillouin zone by *ab initio* density functional theory (DFT). We have characterized the pressure and temperature dependence of the phonon spectrum using the inelastic neutron-scattering technique and performed extensive *ab initio* lattice dynamics calculations of H_2O and D_2O ice in the I*h* phase. We are able to derive the thermal expansion at low temperature from the experimental phonon spectrum. The results bring out the nature of specific anharmonic soft phonon modes that show anomalous behavior as a function of pressure and temperature, which leads to the anomalous thermal expansion behavior of ice. We have thus provided an explanation of the physical mechanism behind the anomalous thermal expansion in ice I*h*. Earlier papers [42,43] report DFT calculations of the negative expansion in ice, but

do not identify the detailed physical picture of the distortion of hexagonal rings that explains the anomalous expansion of ice at low temperature. The calculations are performed in the ordered equivalent structure [44].These calculations reproduce fairly well the experimentally observed anharmonicity of the low-energy phonons, which indicates that effect of the disorder is not very significant in the present context.

II. EXPERIMENTAL

The inelastic spectrum of H_2O and D_2O ice in the I*h* phase were measured on the polycrystalline samples. The measurements were performed at the MERLIN time-of-flight spectrometer at the ISIS facility. The spectrometer is equipped with a large detector bank covering a wide range of about 20° to 120° of scattering angle. High-pressure inelastic neutron-scattering experiments have been carried out on polycrystalline sample of I*h* phase of D_2O. The polycrystalline sample was compressed using argon gas in a gas pressure cell at different pressures of 0, 0.3, and 1 kbar at 225 K. An incident neutron energy of 15 meV is chosen, and the measurements are performed in the energy loss mode. The inelastic neutron-scattering signal is corrected for the contributions from argon at the respective pressures, absorption from the sample, and for the empty cell.

For temperature dependence, we have used about 1-mm- and 2-mm-thick polycrystalline samples for measurement of the spectra from H_2O and D_2O ice, respectively. We have performed measurements at 10, 100, 175, and 225 K using two different incident neutron energies of 15 meV and 55 meV, respectively. In the incoherent one-phonon approximation [45,46], the measured scattering function $S(Q,E)$, as observed in the neutron experiments, is related to the phonon density of states $g^{(n)}(E)$ as follows:

$$g^{(n)}(E) = A\left\langle \frac{e^{2W(Q)}}{Q^2} \frac{E}{n(E,T) + \frac{1}{2} \pm \frac{1}{2}} S(Q,E) \right\rangle, \quad (1)$$

$$g^{n}(E) = B \sum_k \left\{ \frac{4\pi b_k^2}{m_k} \right\} g_k(E), \quad (2)$$

where the + or − signs correspond to energy loss or gain of the neutrons, respectively, and $n(E,T) = [\exp(E/k_BT) - 1]^{-1}$. A and B are normalization constants. b_k, m_k, and $g_k(E)$ are, respectively, the neutron-scattering length, mass, and partial density of states of the k^{th} atom in the unit cell. The quantity between $\langle\rangle$ represents the suitable average over all Q values at a given energy. $2W(Q)$ is the Debye-Waller factor averaged over all the atoms. The weighting factors $\frac{4\pi b_k^2}{m_k}$ in the units of barns/amu for H, D, and O are 82.02, 3.82, and 0.2645, respectively. The values of neutron-scattering lengths for various atoms can be found from Ref. [47].

III. COMPUTATIONAL DETAILS

The phonon calculations of H_2O and D_2O are performed in I*h* phase using the *ab initio* density functional theory as implemented in the VASP software [48,49]. The compounds are known to exhibit H/D disorder, hence the calculations are performed in order to find the equivalent structure I*h* phase, which is a $\sqrt{3} \times \sqrt{3} \times 1$ supercell (space group $P6_3cm$) of the actual unit cell [44]. We note that the space group ($Cmc2_1$) of ice XI is different [50]. The required force constants were computed within the Hellman-Feynman framework, on various atoms in different configurations of a supercell with $(\pm x, \pm y, \pm z)$ atomic displacement patterns. A supercell of $(2 \times 2 \times 2)$, dimension of order equivalent cell, which consists of 96 H_2O molecule has been used in the computations. An energy cutoff of 900 eV was used for plane wave expansion. The Monkhorst Pack method is used for k-point generation [35] with a $4 \times 4 \times 4k$-point mesh was used. The van der Waals (vdW) interaction has been included using the vdW-DFT method [51]. The valence electronic configurations of H and O, as used in calculations for pseudopotential generation are $1s^1$ and s^2p^4, respectively. The convergence breakdown criteria for the total energy and ionic loops were set to 10^{-8} eV and 10^{-4} eV Å^{-1}, respectively. We have used PHONON software [52] to obtained the phonon frequencies in the entire Brillouin zone, as a subsequent step to density functional theory total-energy calculations using the VASP [48,49,53] software. The calculation of the D_2O compound has been carried out using the same pseudopotential as used in H_2O compound. We have tried the structural optimization with all the vdW functionals available in VASP. We found that the vdW functional by Dion *et al.* [8], namely, the DRSLL [41] with revised Perdew-Burke-Ernzerhof (revPBE) functional, gives the closest structure and dynamical properties of ice Ih. Hence, we have used this functional for our calculations.

The thermal expansion behavior has been computed under the quasiharmonic approximation. Each phonon mode of energy E_{qj} (j^{th} phonon mode at point q in the Brillouin zone) contributes to the thermal expansion coefficient, which is given by following relation for a hexagonal system:

$$\alpha_a(T) = \frac{1}{V_0} \sum_{q,j} C_v(q,j,T)[s_{11}\Gamma_a(E_{q,j}) + s_{12}\Gamma_b(E_{q,j}) + s_{13}\Gamma_c(E_{q,j})], \quad (3)$$

$$\alpha_c(T) = \frac{1}{V_0} \sum_{q,j} C_v(q,j,T)[s_{31}\Gamma_a(E_{q,j}) + s_{32}\Gamma_b(E_{q,j}) + s_{33}\Gamma_c(E_{q,j})], \quad (4)$$

where V_0 is the unit-cell volume, Γ_a, Γ_b, and Γ_c are the anisotropic mode Grüneisen parameters. In a hexagonal system, Grüneisen parameters $\Gamma_a = \Gamma_b$. The mode Grüneisen parameter of phonon of energy $E_{q,j}$ is given as [54]

$$\Gamma_l(E_{q,j}) = -\left(\frac{\partial ln E_{q,j}}{\partial ln l}\right)_{l'}; \quad l, l' = a, c. \quad (5)$$

Here s_{ij} are elements of elastic compliances matrix $s = C^{-1}$. $C_v(q,j,T)$ is the specific-heat contribution of the phonons of energy $E_{q,j}$.

The volume thermal expansion coefficient for a hexagonal system is given by

$$\alpha_V = (2\alpha_a + \alpha_c). \quad (6)$$

We have calculated the lattice-parameter dependence of the phonon frequencies and obtained the Grüneisen parameters at 0 K under the quasiharmonic approximation (QHA). These Grüneisen parameters are then used to compute the contribution to the thermal expansion coefficient (α) from phonons of energy E in the entire Brillouin zone at a given temperature T. The calculation includes the phonon contribution at different temperatures through the changes in the phonon population, and the contribution of phonons to the temperature-dependent specific heat. The procedure is equivalent to minimizing the Helmholtz free energy with respect to volume at a finite temperature in the QHA.

IV. RESULTS AND DISCUSSION

A. Phonon Spectrum

We have measured (Fig. 1) the phonon spectra in I*h* phase of D_2O ice at 0, 0.3, and 1.0 kbar (at 225 K) well below the phase transition pressure of about 2 kbar at 225 K where ice I*h* transforms to ice II. The low incident neutron energy of 15 meV ensured the good resolution for the low-energy phonon required to obtain the Grüneisen parameters of phonon modes. The spectrum up to 4 meV clearly shows the Debye like behavior and a peak at ∼7 meV. The basic chracteristics of the low-energy peak is in good agreement with previous measurements [38]. With an increase of pressure, the low-energy phonon modes soften and shift to lower energies. This gives rise to negative Grüneisen parameters for these modes resulting in negative volume thermal expansion at low temperature. The present results on the pressure dependence of the phonon density of states are consistent with an earlier report of phonon dispersion relation along selected directions in the Brillouin zone on ice I*h* performed by Strassle *et al.* [14], which shows the softening of low-energy phonon modes with pressure. Using standard methods as described in Refs. [55–57], the pressure dependence of phonon spectrum is used to obtain the Grüneisen parameter, which is further used to estimate (inset in Fig. 2) the contribution of phonons

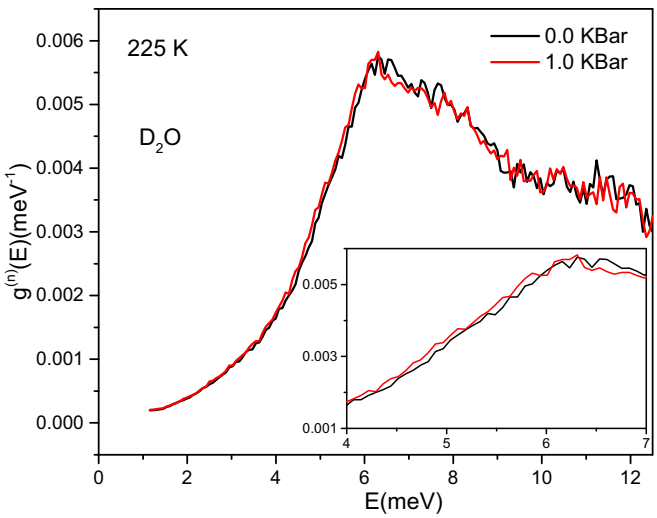

FIG. 1. The low-energy part of experimental phonon spectra, in the I*h* phase of D_2O ice, as a function of pressure. Additional data at 0.3 kbar is given in Fig. SII [58].

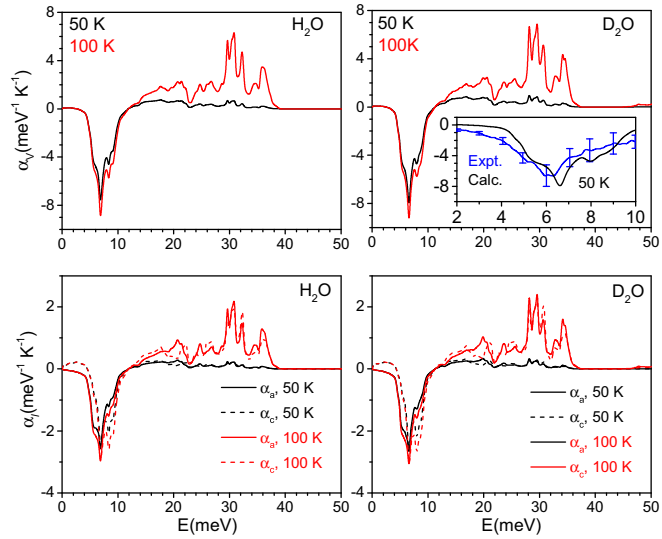

FIG. 2. The *ab initio* calculated contribution to the volume (Top panel) and linear (Bottom panel) thermal expansion coefficient from phonons of energy E averaged over entire Brillouin zone at $T = 50$ K and 100 K. Inset shows the volume thermal expansion coefficient as a function of phonon energy in D_2O ice as obtained from pressure dependence of neutron inelastic measurements and comparison with the calculation.

of energy E to the volume thermal expansion coefficient at 50 K. It can be seen that phonons of energy around 6 meV contribute the most to the observed NTE behavior. As shown below, this observation is in excellent agreement with our *ab initio* calculations.

We have measured (Fig. 3) the inelastic neutron spectrum at temperatures ranging from 10 to 225 K for H_2O and D_2O in the I*h* phase. The measurements are performed with two incident neutron energies of 15 and 55 meV. The 15-meV-incident neutrons give inelastic scattering data up to about 12 meV with very good resolution ($\Delta E \sim 0.6$ meV at elastic line); with 55 meV incident neutrons we can obtain inelastic scattering data up to 45 meV of moderate resolution ($\Delta E \sim$ 2.45 meV). The spectrum show sharp peaks at about 7, 20, 28, and 38 meV in both the compounds. The low-energy modes around 6 meV show softening with increase in temperature which can be clearly seen in both the compounds. This is characteristic of the presence of anharmonic phonon modes. The measured inelastic spectrum shows broadening of various peaks at higher temperature, which arises due to the anharmonic nature of the phonons as well as an increase in H/D disorder with temperaure. At high temperature (∼225 K) the signature of H/D disorder dominates and the sharp peak-like features of the spectrum disappear.

The calculated neutron-weighted phonon density of states compared with the measurements is shown in Fig 3. The calculation agrees fairly well with the measurements at low temperature at 10 K. However, the peaks at 28 and 38 meV in the experimental data are slightly overestimated and underestimated respectively in the calculated spectra. The negative expansion behavior occurs below 60 K and the contributions of high-energy modes is not very significant at such low temperatures, which gives us confindence to understand the

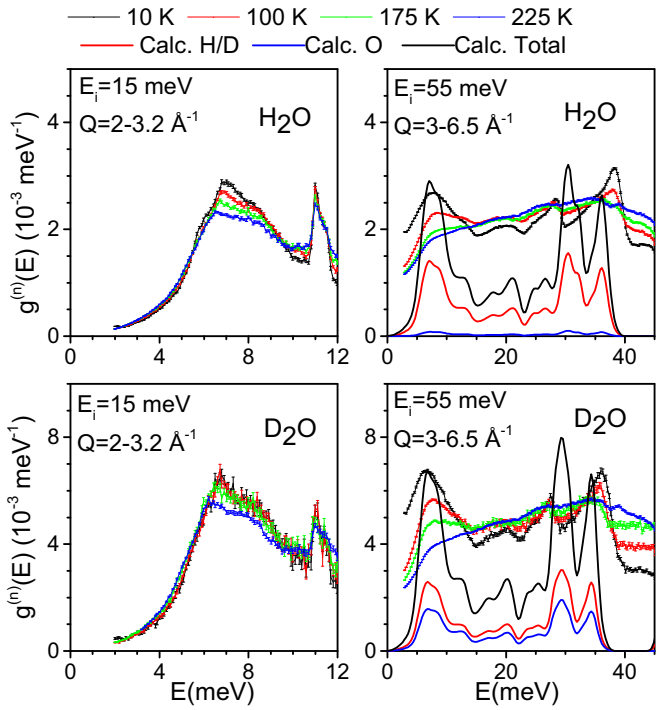

FIG. 3. The low-energy part of experimental phonon spectra, in the I*h* phase of H_2O and D_2O ice, as a function of temperature. The data are collected with two incident neutron energies of 15 and 55 meV. The calculated neutron weighted phonon spectra as well as partial phonon contributions of H/D and O atoms are also shown. For clarity, the experimental data is vertically shifted.

anamolous behavior of H_2O and D_2O in the I*h* phase with the current computational formalism. An examination of the calculated phonon eigenvectors shows that the modes below 40 meV are essentially the translational modes of H_2O/D_2O molecules. The calculated neutron cross section weighted partial phonon density of states shows (Fig. 3) that at low energies, the experimental neutron spectrum in H_2O ice is dominated by H atoms due to the large incoherent cross section of H. However in the experimental neutron spectra of D_2O ice, both the D and O atoms have comparable contributions.

B. Thermal Expansion Behavior

In order to calculate the thermal expansion behavior, we need to have Grüniesen parameters as derived from pressure dependence of phonon frequencies. The pressure dependence of phonon dispersion relation along various high-symmetry direction is shown in Fig. 4. We obtained the softening of low-energy modes below 12 meV on compression from the calculations. Further we have also calculated the phonon frequencies on anisotropic compression along the a and c axes. Table I shows the calculated Grüneisen parameters (Γ_a, Γ_c, and Γ_V) of a few selected phonon modes of about 6 meV.The anisotropic compression along the c axis shows (Fig. 5) that phonon modes below 2 meV have positive Grüneisen parameters (Γ_c).

Since lowering of the phonon frequency would enhance the entropy, these phonon modes (<12 meV) act to reduce

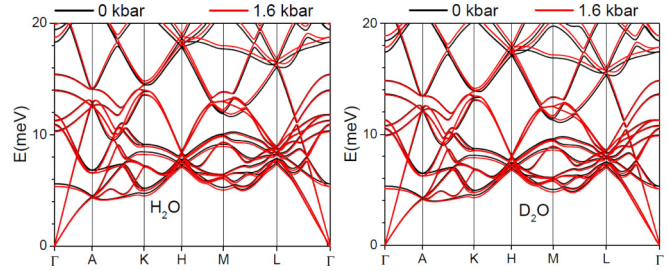

FIG. 4. The calculated pressure dependence of the phonon dispersion of H_2O and D_2O ice in I*h* phase. For better visibility the phonon energies are shown up to 20 meV.

the volume of the system. However, the energy of other higher-energy modes increases on compression which would decrease the entropy. These modes will not favor volume contraction and instead work to expand the lattice. The competition between these two regimes of phonon modes and their population govern the overall thermal expansion behavior. At low temperature (<60 K) only the low-energy modes are populated significantly. The other high-energy modes are not sufficiently populated to compete with these low-energy modes. Hence D_2O/H_2O ice I*h* shows negative thermal expansion behavior at low temperature (Fig. 6). Further, at high temperature above 60 K the high-energy modes above 12 meV start populating significantly and dominate, which leads to positive expansion behavior.

Since the hexagonal structure of the I*h* phase is anisotropic, we have calculated the anisotropic linear thermal expansion (Fig. 6). The behavior of linear expansion coefficients (α_a and α_c) are related to anisotropic Grüneisen parameters (Γ_a and Γ_c) as well as the elastic compliance matrix [Eqs. (3) and (4)]. The elastic compliance matrix shows (Table SIV [58]) that compressibilities along the a and c axes are very similar, also the anisotropic Grüneisen parameter (Γ_a and Γ_c) behavior is very similar (Fig. 5). Hence only the negative magnitude of

TABLE I. The calculated anisotropic Grüneisen parameter of a few phonons having large Grüneisen parameters in the Brillouin zone of an ordered analogue (space group $P6_3cm$) of ice I*h*. *E* and Γ are the energy and Grüneisen parameter, respectively. The wave vectors are Γ(0 0 0), A(0 0 0.5), K(.33 0.33 0), H(.33 0.33 0.5), M(0.5 0.5 0), and L(0.5 0.5 0.5)

Wave vector	E(meV)	Γ_a	Γ_c	Γ_V
		H_2O/D_2O		
Γ	5.6/5.3	−2.0/−2.0	−5.3/−5.2	−3.1/−3.0
A	4.5/4.2	−0.9/−0.9	−3.7/−3.6	−1.9/−1.8
A	6.8/6.5	−3.0/−3.1	−2.9/−2.8	−3.0/−3.0
K	4.7/4.5	−4.0/−3.9	−3.0/−2.7	−3.7/−3.5
K	5.2/4.9	−2.9/−2.9	−1.6/−1.4	−2.5/−2.4
K	7.1/6.8	−0.5/−0.5	−0.7/0.7	−0.6/0.6
H	7.3/6.9	−1.6/−1.5	−1.5/−1.5	−1.6/−1.5
H	7.7/7.4	−1.6/−1.7	−1.6/−1.7	−1.6/−1.7
M	5.3/5.0	−3.9/−4.0	−2.1/−2.2	−3.4/−3.4
M	6.1/5.8	−0.5/−0.5	−0.2/−0.2	−0.4/−0.4
L	7.5/7.2	−1.6/−1.5	−1.6/−1.7	−1.6/−1.6
L	7.8/7.5	−1.6/−1.6	−1.4/−1.4	−1.5/−1.5

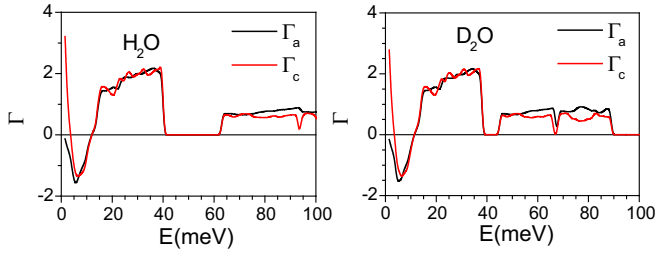

FIG. 5. The calculated anisotropic Grüneisen parameters in the I*h* phase of H_2O and D_2O ice.

the Grüneisen parameter will give rise to negative expansion behavior at low temperature.

The experimental measurements [12,13] of thermal expansion behavior show that magnitude of NTE below 40 K in D_2O ice is slightly more in comparison to H_2O ice, while at high temperature the magnitude of positive thermal expansion behavior in D_2O ice is larger than that in H_2O ice (Figs. 6 and 7). This can be understood from the calculated partial and total phonon spectrum. The negative thermal expansion is contributed by low-energy phonon modes below 12 meV. The partial and total phonon spectrum looks very similar (Fig. SIII) in both the cases [58]. However, due to mass effect the lowest peak at about 7 meV in density of states in H_2O is shifted to slightly lower energies at about 6.5 meV.

The nature of Grüneisen parameters show a negative sign below 12 meV and afterward it is positive. Indeed, the positive or the negative thermal expansion is determined by the product of the compliance tensor components and the anisotropic Grüneisen parameters of modes that are populated at the temperature of interest. The NTE could indeed arise from negative compliance tensor components or negative Grüneisen parameters. In the present case, we find that the Grüneisen parameters are almost isotropic, $\Gamma_a = \Gamma_b \approx \Gamma_c$ and therefore, we can simply rewrite the Eqs. (3) and (4) using elastic compliance tensor values as $\alpha_a(T) \propto \sum_{q,j} C_v(q,j,T)[0.00248\Gamma_a(E_{q,j})]$ and $\alpha_c(T) \propto \sum_{q,j} C_v(q,j,T)[0.00236\Gamma_a(E_{q,j})]$. This clearly shows that the thermal expansion coefficients as a function of temperature essentially follow the Grüneisen parameters and the phonon population, since the compliance tensor terms add up to a positive number. Hence the expansion behavior along both the a and c axes shows negative expansion behavior at low temperature (<60 K) and after that it shows positive expansion behavior.

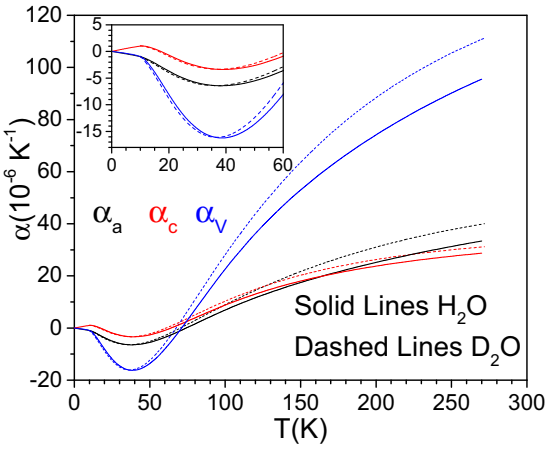

FIG. 6. The calculated linear and volume thermal expansion coefficients the I*h* phase of H_2O and D_2O ice.

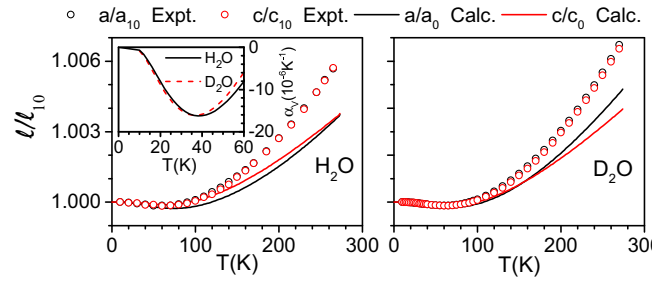

FIG. 7. The calculated and measured [13] lattice parameter change (l/l_{10}; l = a, c) of ice with temperature. Inset in the left panel shows the calculated volume thermal expansion coefficient (α_v) of H_2O and D_2O ice up to 60 K.

The calculated fractional change in the lattice parameters with temperature shows excellent agreement with the available measurements [13] at temperature below 100 K (Fig. 7). At temperature around 200 K, the calculated thermal expansion behavior is underestimated in comparion to the experimental data. We note that the experimental bulk modulus value of H_2O Ice in I*h* phase is known to show large variation from 10.5 to 8.3 GPa on increase of temperature from 60 K to 270 K. The increase in the compressibility or the elastic compliance tensor would lead to an increase in the thermal expansion. Our *ab initio* calculations are performed using QHA at 0 K. For thermal expansion calculation, we used the elastic compliance tensor as calculated from DFT at 0 K,which means that some of the elastic compliance component would increase singnificantly with temperature and would be responsible for increase in positive expansion behavior at high temperature. The present formalism of the calculation of thermal expansion behavior does not account for this effect, and may lead to underestimation of calculated volume thermal expansion at higher temperature. This essentially reflects the limitation of QHA in the present case [59]. The magnitude of positive expansion in D_2O (Fig. 7) is larger than that in H_2O, which is due to the fact that high-energy phonon modes that contribute to positive expansion are shifted towards the lower energy side due to the heavy mass of D; hence they are excited at lower temperature and add to the extra postive expansion in comparision to H_2O.

In order to estimate the phonons which contribute mainly to positive and negative expansion behavior, the calculated pressure dependence of phonon energies are used to estimate the thermal expansion coefficient as a function of phonon energy (Fig. 2) averaged over the entire Brillouin zone at 50 K. Interestingly we find that phonon modes below 12 meV give rise to a negative linear expansion coefficient. The high-energy phonons (in the range from 12 to 40 meV) contribute to very a small positive contribution resulting in overall NTE behavior. However with increase of temperature to 100 K, the negative contribution by phonon of energy below 12 meV

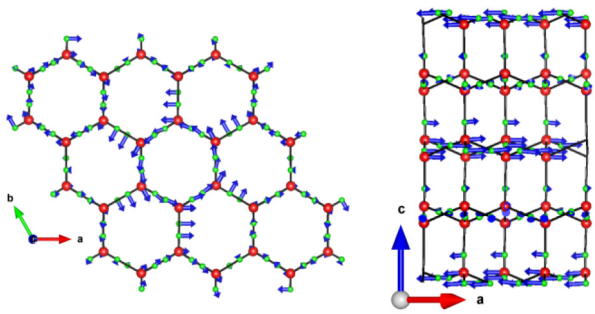

K-point
H_2O: 4.7 meV, -4.0, -3.0, -3.7
D_2O: 4.5 meV, -3.9, -2.7, -3.5

A-point
H_2O: 4.5 meV, -0.9, -3.7, -1.9
D_2O: 4.2 meV, -0.9, -3.6, -1.8

FIG. 8. The atomic displacement pattern of selected phonon modes of H_2O/D_2O in I*h* phase of ice. The number below the figure gives the phonon energies, Γ_a, Γ_c, and Γ_V, respectively. Key- H/D: Green and O: Red.

does not change significanly. The additional large positive contribution from high-energy modes is enhanced singnificantly and also contributes to the total thermal expansion resulting in overall large positive expansion. The *ab initio* calculations and observations from high-pressure experiments (inset in Fig. 2) at 50 K are found to be in excellent agreement.

As discussed above, low-energy phonon modes below 12 meV contribute to negative expansion in both the I*h* phase of ice D_2O and H_2O. In Table I, we have given the Grüneisen parameters of a few selected phonon modes relevent to NTE behavior in the compound. However the nature of the dynamics .i.e. the atomic motion pattern for such modes have not been known. In order to visualize these dynamics we have drawn the atomic displacement pattern of one representative phonon mode which contributesto NTE (Fig. 8).

The displacement pattern of the *K*-point phonon mode of 4.7 meV energy is shown in Fig. 8; this manifests itself as a rotational motion of the hexagonal rings and a distortion of the ring structure, which acts to reduce the area of the rings and thereby give rise to NTE in the a-b plane. The hexagonal rings, arranged into sheets, are stacked along the c direction. The cooperative rotation of the hexagonal rings in one plane influences, due to polyhedral connectivity of the H bonds, the interplanar separation. Another mode (Fig. 8) of similar energy ∼4.5 meV at the A-point involves transverse vibrations of the hexagonal layers, which further contributes to NTE along the c axis. These calculations show that it is the rotational dynamics of the hexagonal rings that leads to NTE in these ice. Animations of a few selected modes are given in the Supplemental Material [58].

V. CONCLUSIONS

In this paper, we have quantitatively derived the anisotropic and anomalous thermal expansion in H_2O and D_2O ice in the I*h* phase. This has also enabled us to understand the quantitative difference in thermal expansion behavior of the H_2O and D_2O ice. The inelastic neutron-scattering measurements of the pressure dependence of phonon density of states of deuterated ice (D_2O) reveal a pronounced softening of low-energy anharmonic modes. The increase in broadening of the peaks in the temperature dependence of phonon spectra of both the protonated (H_2O) and deuterated ice (D_2O) indicates increase in disorder of H/D atoms with increasing temperature. Using the *ab initio* density functional theory we have identified the nature of specific anharmonic phonons, namely, the librational motion of the hexagonal rings of the ice molecules and the transverse vibrations of the hexagonal layers that lead to the observed behavior in ice.

ACKNOWLEDGMENTS

S.L.C. would thanks the Department of Atomic Energy, India for the award of the Raja Ramanna Fellowship. The use of the ANUPAM supercomputing facility at BARC is acknowledged. The authors also thank STFC, United Kingdom for the beam-time at ISIS and thank the pressure and furnace section technicians for their essential assistance in setting up the equipment.

[1] V. F. Petrenko and R. W. Whitworth, *Physics of Ice* (Oxford University Press, Oxford, UK, 1999).
[2] E. A. Engel, Y. Li, and R. J. Needs, Phys. Rev. B **97**, 054312 (2018).
[3] B. Pamuk, P. B. Allen, and M. V. Fernández-Serra, Phys. Rev. B **92**, 134105 (2015).
[4] B. Pamuk, J. M. Soler, R. Ramírez, C. P. Herrero, P. W. Stephens, P. B. Allen, and M. V. Fernández-Serra, Phys. Rev. Lett. **108**, 193003 (2012).
[5] K. Kobayashi, M. Koshino, and K. Suenaga, Phys. Rev. Lett. **106**, 206101 (2011).
[6] N. H. Fletcher, *The Chemical Physics of Ice* (Cambridge University Press, Cambridge, 2009).
[7] C. G. Salzmann, P. G. Radaelli, A. Hallbrucker, E. Mayer, and J. L. Finney, Science **311**, 1758 (2006).
[8] E. B. Moore and V. Molinero, Nature (London) **479**, 506 (2011).
[9] O. Mishima and H. E. Stanley, Nature (London) **396**, 329 (1998).
[10] L. E. Bove, S. Klotz, J. Philippe, and A. M. Saitta, Phys. Rev. Lett. **106**, 125701 (2011).
[11] C. Fang, W.-F. Li, R. S. Koster, J. Klimes, A. van Blaaderen, and M. A. van Huis, Phys. Chem. Chem. Phys. **17**, 365 (2015).
[12] K. Rottger, A. Endriss, J. Ihringer, S. Doyle, and W. F. Kuhs, Acta Crystallog. Sec. B **50**, 644 (1994).
[13] A. D. Fortes, Acta Crystallog. Sec. B **74**, 196 (2018).
[14] T. Strässle, A. M. Saitta, S. Klotz, and M. Braden, Phys. Rev. Lett. **93**, 225901 (2004).
[15] M. M. Koza, Phys. Rev. B **78**, 064303 (2008).
[16] M. M. Koza, B. Geil, K. Winkel, C. Köhler, F. Czeschka, M. Scheuermann, H. Schober, and T. Hansen, Phys. Rev. Lett. **94**, 125506 (2005).
[17] M. M. Koza, H. Schober, S. F. Parker, and J. Peters, Phys. Rev. B **77**, 104306 (2008).

[18] P. Gallo, K. Amann-Winkel, C. A. Angell, M. A. Anisimov, F. Caupin, C. Chakravarty, E. Lascaris, T. Loerting, A. Z. Panagiotopoulos, J. Russo, J. A. Sellberg, H. E. Stanley, H. Tanaka, C. Vega, L. Xu, and L. G. M. Pettersson, Chemical Reviews **116**, 7463 (2016).
[19] E. A. Engel, B. Monserrat, and R. J. Needs, J. Chem. Phys. **143**, 244708 (2015).
[20] E. A. Engel, B. Monserrat, and R. J. Needs, Phys. Rev. X **5**, 021033 (2015).
[21] F. Yen and T. Gao, J. Phys. Chem. Lett. **6**, 2822 (2015).
[22] P. Zhang, L. Tian, Z. P. Zhang, G. Shao, and J. C. Li, J. Chem. Phys. **137**, 044504 (2012).
[23] L. Tian, A. I. Kolesnikov, and J. Li, J. Chem. Phys. **137**, 204507 (2012).
[24] A. Putrino and M. Parrinello, Phys. Rev. Lett. **88**, 176401 (2002).
[25] M. Benoit, M. Bernasconi, P. Focher, and M. Parrinello, Phys. Rev. Lett. **76**, 2934 (1996).
[26] P. Demontis, R. LeSar, and M. L. Klein, Phys. Rev. Lett. **60**, 2284 (1988).
[27] A. Polian and M. Grimsditch, Phys. Rev. Lett. **52**, 1312 (1984).
[28] C. Bellin, B. Barbiellini, S. Klotz, T. Buslaps, G. Rousse, T. Strässle, and A. Shukla, Phys. Rev. B **83**, 094117 (2011).
[29] T. Strässle, A. Caviezel, B. Padmanabhan, V. Y. Pomjakushin, and S. Klotz, Phys. Rev. B **82**, 094103 (2010).
[30] S. Klotz, L. E. Bove, T. Strässle, T. C. Hansen, and A. M. Saitta, Nat. Mater. **8**, 405 (2009).
[31] T. Strässle, S. Klotz, G. Hamel, M. M. Koza, and H. Schober, Phys. Rev. Lett. **99**, 175501 (2007).
[32] R. J. Nelmes, J. S. Loveday, T. Strässle, C. L. Bull, M. Guthrie, G. Hamel, and S. Klotz, Nature (London) Physics **2**, 414 (2006).
[33] Th. Strässle, S. Klotz, J. S. Loveday, and M. Braden, J. Phys.: Condens. Matter **17**, S3029 (2005).
[34] B. Minceva-Sukarova, W. F. Sherman, and G. R. Wilkinson, J. Phys. C: Solid State Phys. **17**, 5833 (1984).
[35] M. Zhang, H. Xu, E. K. H. Salje, and P. J. Heaney, Phys. Chem. Miner. **30**, 457 (2003).
[36] T. Shigenari and K. Abe, J. Chem. Phys. **136**, 174504 (2012).
[37] F. Perakis, S. Widmer, and P. Hamm, J. Chem. Phys. **134**, 204505 (2011).
[38] J. Li, J. Chem. Phys. **105**, 6733 (1996).
[39] B. Pamuk, P. B. Allen, and M.-V. Fernández-Serra, J. Phys. Chem. B **122**, 5694 (2018).
[40] É. D. Murray and G. Galli, Phys. Rev. Lett. **108**, 105502 (2012).
[41] I. Presiado, J. Lal, E. Mamontov, A. I. Kolesnikov, and D. Huppert, J. Phys. Chem. C **115**, 10245 (2011).
[42] Z.-K. Liu, Y. Wang, and S. Shang, Sci. Rep. **4**, 7043 (2014).
[43] M. A. Salim, S. Y. Willow, and S. Hirata, J. Chem. Phys. **144**, 204503 (2016).
[44] J. D. Bernal and R. H. Fowler, J. Chem. Phys. **1**, 515 (1933).
[45] J. M. Carpenter and D. L. Price, Phys. Rev. Lett. **54**, 441 (1985).
[46] D. L. Price and K. Skold, *Neutron Scattering* (Academic Press, Orlando, 1986).
[47] V. F. Sears, Neutron News **3**, 26 (1992).
[48] G. Kresse and J. Furthmüller, Phys. Rev. B **54**, 11169 (1996).
[49] G. Kresse and D. Joubert, Phys. Rev. B **59**, 1758 (1999).
[50] C. M. B. Line and R. W. Whitworth, J. Chem. Phys. **104**, 10008 (1996).
[51] M. Dion, H. Rydberg, E. Schröder, D. C. Langreth, and B. I. Lundqvist, Phys. Rev. Lett. **92**, 246401 (2004).
[52] PHONON software, K. Parlinksi, 2003.
[53] G. Kresse and J. Furthmüller, Comput. Mater. Sci. **6**, 15 (1996).
[54] E. Grüneisen and E. Goens, Z. Phys. **29**, 141 (1924).
[55] R. Mittal, M. K. Gupta, and S. L. Chaplot, Prog. Mater. Sci. **92**, 360 (2018).
[56] M. K. Gupta, B. Singh, R. Mittal, M. Zbiri, A. B. Cairns, A. L. Goodwin, H. Schober, and S. L. Chaplot, Phys. Rev. B **96**, 214303 (2017).
[57] R. Mittal, S. L. Chaplot, H. Schober, and T. A. Mary, Phys. Rev. Lett. **86**, 4692 (2001).
[58] See Supplemental Material at http://link.aps.org/supplemental/10.1103/PhysRevB.98.104301 for details of partial phonon density of states, elastic constants, compliance, and animation of low-energy modes at ambient pressure.
[59] L. Monacelli, I. Errea, M. Calandra, and F. Mauri, Phys. Rev. B **98**, 024106 (2018).